Modeling large patterned deflection during lithiation of micro-structured silicon

Alexander M. Laptev [a,*], Yohanes C. Malede [a], Shanghong Duan [a], Robert Mücke [a], Dmitry Danilov [b], Peter H. L. Notten [b,c], Olivier Guillon [a]

[a] Jülich Aachen Research Alliance: JARA-Energy, Institute of Energy and Climate Research, Materials Synthesis and Processing (IEK-1), Forschungszentrum Jülich GmbH, 52425 Jülich, Germany
Laptev@gmx.net, YMalede@gmail.com, S.Duan@fz-juelich.de, R.Muecke@fz-juelich.de, , O.Guillon@fz-juelich.de

[b] Department of Chemical Engineering and Chemistry, Eindhoven University of Technology, 5600 MB Eindhoven, The Netherlands
D.Danilov@tue.nl, P.H.L.Notten@tue.nl

[c] Jülich Aachen Research Alliance: JARA-Energy, Institute of Energy and Climate Research, Fundamental Electrochemistry (IEK-9), Forschungszentrum Jülich GmbH, 52425 Jülich, Germany

[*] Corresponding author. E-mail address: laptev@gmx.net (A. M. Laptev)

Abstract

The application of silicon (Si) as potential anode material in Li-ion batteries provides a more than nine-fold increase in gravimetric storage capacity compared to conventional graphite anodes. However, full lithiation of Si induces the volume to increase by approximately 300%. Such enormous volume expansion causes large mechanical stress, resulting in non-elastic deformation and crack formation. This ultimately leads to anode failure and strong decrease in cycle life. This problem can be resolved by making use of structured anodes with small dimensions. Particularly honeycomb-shaped microstructures turned out to be beneficial in this respect. In the present paper, finite element modeling was applied to describe the experimentally observed mechanical deformation of honeycomb-structured Si anodes upon lithiation. A close agreement between simulated and experimentally observed shape changes is observed in all cases. The predictive ability of the model was further exploited by investigating alternative geometries, such as square-based microstructure. Strikingly, dimension and pattern optimization shows that the stress levels can be reduced even below the yield strength, while maintaining the footprint-area-specific storage capacity of the microstructures. The pure elastic deformation is highly beneficial for the fatigue resistance of optimized silicon structures. The obtained results are directly applicable for other (de)lithiating materials, such as mixed ionic-electronic conductors (MIEC) widely applied in Li-ion and future Na-ion batteries.

Keywords: Silicon anode; Honeycomb; Lithiation; Volumetric expansion; Patterned deformation; Chemo-mechanics; Finite element analysis

1. Introduction

Nowadays the application area of rechargeable Li-ion batteries expands rapidly. On the one hand, drug delivery systems, microelectronic sensors and smart cards demand micro-size batteries while, on the other hand, automotive applications and residential storage require battery packs are required on the kWh and even MWh scale. Silicon is an interesting anode material for Li-ion batteries because of its high storage capacity and fast charge transfer kinetics. Though the development of Si-based anode materials started already some while ago, considerable challenges are still lying ahead.

Silicon shows huge volume changes during charging (lithiation) and discharging (delithiation). Consequently, the Si anodes experience fast degradation during cycling [1,2]. Nano-structuring has fairly been considered as a perspective way to improve the cycling life of Si electrodes [3-5]. The simplest way to nano-structure electrodes is in thin films. The cycling performance of Si thin film anodes is good, but the storage capacity per footprint area is rather low [6]. To increase this storage capacity per footprint unit, 3D geometries can be applied, *e.g.* in the form of trenches, pillars and nanowires [7]. Three-dimensional structuring leads to large improvements in storage capacity. However, the stability of materials remains a challenge. To improve the cycling stability new, more robust, 3D architectures have to be developed.

Honeycomb structures have excellent mechanical properties and are widely applied in many constructions from the middle of the XX century onwards [8]. Honeycomb Si structures for Li-ion battery applications have been manufactured and electrochemically investigated, revealing remarkable ordered morphological changes during reversible (de)lithiation (Fig. 1a) [9]. These microstructures may form the basis for the development of new 3D Li-ion battery concepts. The mechanical behavior of honeycomb-structured electrodes is therefore interesting and scientifically challenging to investigate in more detail.

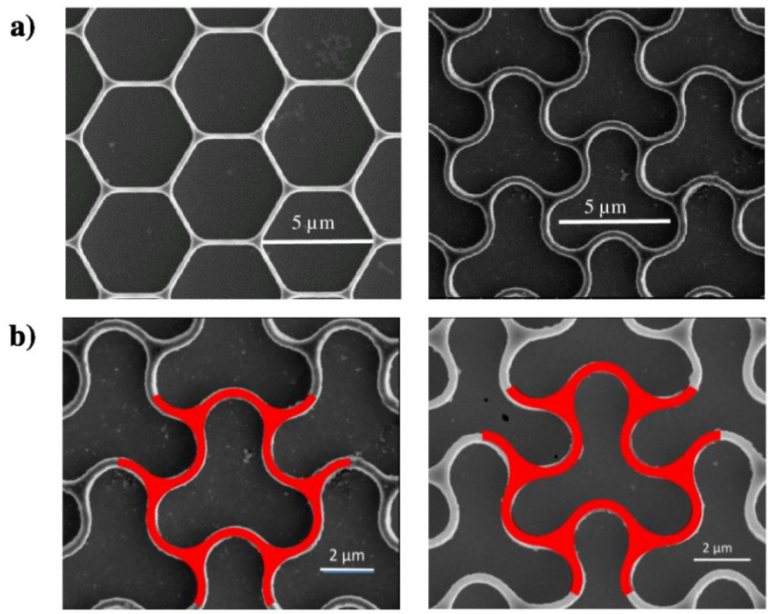

Fig. 1. a) Morphology of honeycomb-structured Si anode before lithiation (left) and after lithiation (right) observed in experiments [9]; b) overlay of experimental and simulated (red) cell patterns: lithium loading of 45 % (left) and 80 % (right).

In the present paper a finite element approach is used to model the deflection of honeycomb-structured Si upon (de)lithiation. The stresses and strains were calculated, taking the dimensions of honeycomb cells and charging conditions identical to those used in the experiments described before [9]. Subsequently, the original honeycomb geometry was optimized to reduce stress levels and eliminate plastic deformation. In addition, a new square-based geometry was proposed and analyzed. The modeling results are compared with experimental data from literature.

2. Theoretical background

The driving force for swelling and deflection of Si-based anodes is the insertion of Li-ions into the Si matrix. Li insertion was modeled as a diffusional flow through the free surface of the honeycomb cells. The further Li storage into the Si matrix and related concentration rise has been modeled by Fick's law, using a diffusion coefficient of $5.1 \cdot 10^{-4}$ $\mu m^2 \cdot s^{-1}$ [10]. Isotropic Si behavior has been assumed. The development of Li-induced linear strain has been described by the linear function

$e^{Li}=\beta_{Li}\cdot C_{Li}$ [11,12], where e^{Li} is the Li-induced Hencky (logarithmic) strain, β_{Li} is the coefficient of linear expansion and C_{Li} is the normalized Li-molar concentration defined as $C_{Li} = x/x_{max}$. x_{max} = 3.75 is the maximal molar amount of Li, which can be stored per mole of Si in the reported $Li_{3.75}Si$ phase [6]. Accordingly, C_{Li} ranges from 0 before charging to 1 for fully charged anodes. The coefficient β_{Li} was determined by formula $\beta_{Li} = e^{Li} = 1/3 \cdot ln(V_{Li}/V_0)$, where V_0 and V_{Li} denote the volume of the Si structure before lithiation and after full lithiation when C_{Li}=1.0. Taking into account the experimentally observed ratio V_{Li}/V_0=3.8 [13], the value of β_{Li}=0.445 was found. The elastoplastic behavior of Si was assumed and an incremental approach was implemented in the structural part of the model. Thus, the total strain increment (de) was defined as the sum of Li-induced (de^{Li}), elastic (de^e) and plastic (de^p) strain increments, *i.e.* $de=de^{Li}+de^e+de^p$. The Young's modulus (E) and Poisson ratio (v) are required to calculate de^e by Hooke's law. According to theoretical considerations and experimental observations, the Young's modulus decreases with increasing Li concentration [14,15]. The linear relationship for the Young's modulus E=90-78$\cdot C_{Li}$ [GPa] was used based on a previous experimental study on Li-Si thin films [15]. The Poisson ratio is weakly affected by the Li content [14]. Therefore, a constant value of v=0.28 was used in the present work. Information on the inelastic behavior of lithiated Si is still limited. It is known that with increasing Li concentration, Si exhibits a brittle-to-ductile transition and a reduction in hardness and strength [16,17]. Both the strength and ductility are strongly affected by the method of material synthesis, obtained microstructure and the presence of defects. In addition, experimental data show a large scattering, even for the same material [16]. In this work we used a linear dependence of the yield strength (σ_Y) on the Li concentration, given by σ_Y=7.2-5.7$\cdot C_{Li}$ [GPa]. This is in line with the modeling results obtained by density function theory [17]. Similar results were reported by first principles theoretical studies and molecular dynamics calculations [18,19]. Using the frequently reported lower values for the Si yield strength [16,20], considerable differences between the modeled and experimentally observed shape of honeycomb cell (*e.g.* the wall buckling) were found.

Perfectly plastic behavior or even softening of lithiated Si was previously theoretically predicted and confirmed by experiments [16-19]. Therefore, the model of a perfectly plastic behavior of Si has been adopted in the present work. The identical yield strength in tension and compression was assumed.

3. Modeling

3.1. Procedure

The model was numerically implemented in ANSYS® 15.0 finite element software (ANSYS Inc., Canonsburg, USA) as an APDL code. The reference honeycomb microstructure with a distance between two vertexes of L=2.9 μm, wall thickness of t=0.25 μm and wall height of h=1.1 μm was adopted from the experimental work of Baggetto *et al*. [9]. The fillet radius between the walls was taken r=0.3 L. The microstructure was supposed to be in mechanical and electrical sliding contact with the underlying conducting substrate. The frictionless displacement has been assumed in view of in-plane loading and small weight of the honeycomb structure. A single representative 2D honeycomb cell with symmetric periodic boundary conditions has been used to model the whole structure. The finite element modeling was based on PLANE 223 element with structural-thermal-diffusional analysis capability. The free meshing option was applied. The geometrical nonlinearity was considered by NLGEOM, ON command. The accuracy in the determination of large deformations was ensured by the incremental FEM approach and by the use of Hencky strain measure on each increment. The formal analogy between thermal and diffusion analysis has been applied to include the concentration dependence of mechanical properties for lithiated silicon.

Galvanostatic charging with a current density of 75 $\mu A \cdot cm^{-2}$ geometric footprint area has been implemented from the experimental work [9]. Prescribed levels of lithiation have been simulated by variation in charging time. During charging, lithium distribution was found to some extent inhomogeneous, with higher concentrations in the honeycomb walls and lower concentrations around

vertexes. However, interrupting charging followed by a subsequent resting period of 1 h provided fully uniform Li concentrations throughout the entire honeycomb structure in all simulations. The honeycomb- and square-shaped microstructures are therefore compared after complete homogenization in Li distribution.

3.2. Results

The simulated evolution of honeycomb deformation upon lithiation is presented in Fig. 2. The honeycomb structure shows an ordered deformation pattern with an increasing degree of bending as the Li amount is augmented. Opposite walls are displaced and curved in the same direction avoiding mutual contact. The distance between two neighboring vertexes was found unchanged. This finding is confirmed by experimental observations. Geometrically stable positions of the vertexes provide additional electrical contacts between the honeycombs and the substrate.

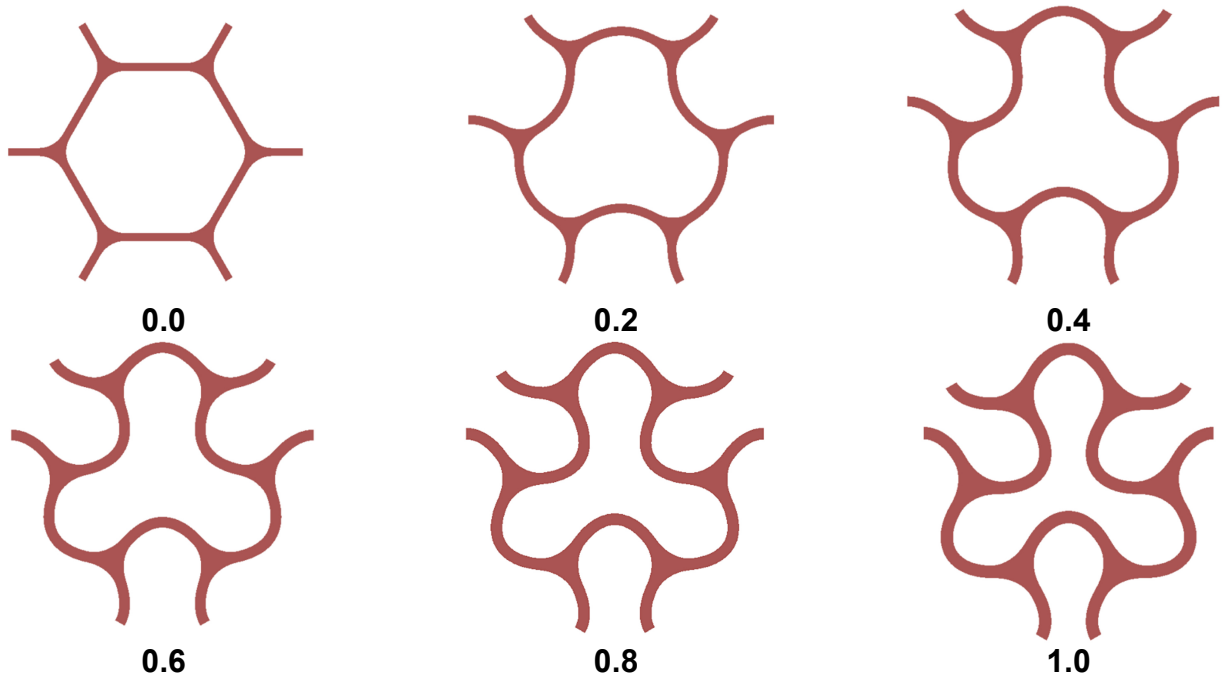

Fig. 2. Modeled evolution of a honeycomb cell with increasing lithium concentration, indicated by the numbers.

The stress and total mechanical strain ($de^{mech}=de^{e}+de^{p}$) distribution across the honeycomb walls is typical for bending with tension and compression regions and neutral axis as shown in Fig. 3a and b. The ductility in tension usually is significantly lower than in compression. Therefore only tensile stress and strain are further discussed. The maximal tensile stress and strain arise on top of the deformed honeycomb walls. Initially, the lithiation induces the elastic strain (Fig. 3c). The plastic strain arises at Li content of about 0.3. During further lithiation, plastic strain increases up to a value of 0.076 at a Li content of 0.8. During this stage the elastic part of strain remains nearly constant. At larger lithiation, an additional increase in elastic strain and unchanged plastic strain occurs. Obviously, the deformation behavior is closely related to the maximal stress development discussed later. Plastic strains are mainly localized in the central part on both sides of the honeycomb walls as shown in Fig. 3d. However, due to localized position and relatively low magnitude, they hardly influence the overall honeycomb configuration. The shape of the bent walls approaches the segmental arch and is mainly determined by the Li amount and the distance between the two vertexes. Nevertheless, subsequent delithiation leads to small residual distortion of the honeycomb walls, residual plastic strain and residual stress in their central part (Fig. 3d). During (de)lithiation cycling, the ductility of Si varies considerably [17]. The initial inelastic strains may therefore result in micro-cracks, leading to a progressive increase in structural damage, thereby shortening the lifetime of Si anodes [21]. It is worthwhile to note that at lower yield strength than used in this study much larger plastic deformations penetrating the walls are predicted. This results in sharp kinks and buckling of the honeycomb walls (Fig. S1). The critical value of the maximal plastic strain was estimated to be 0.1.

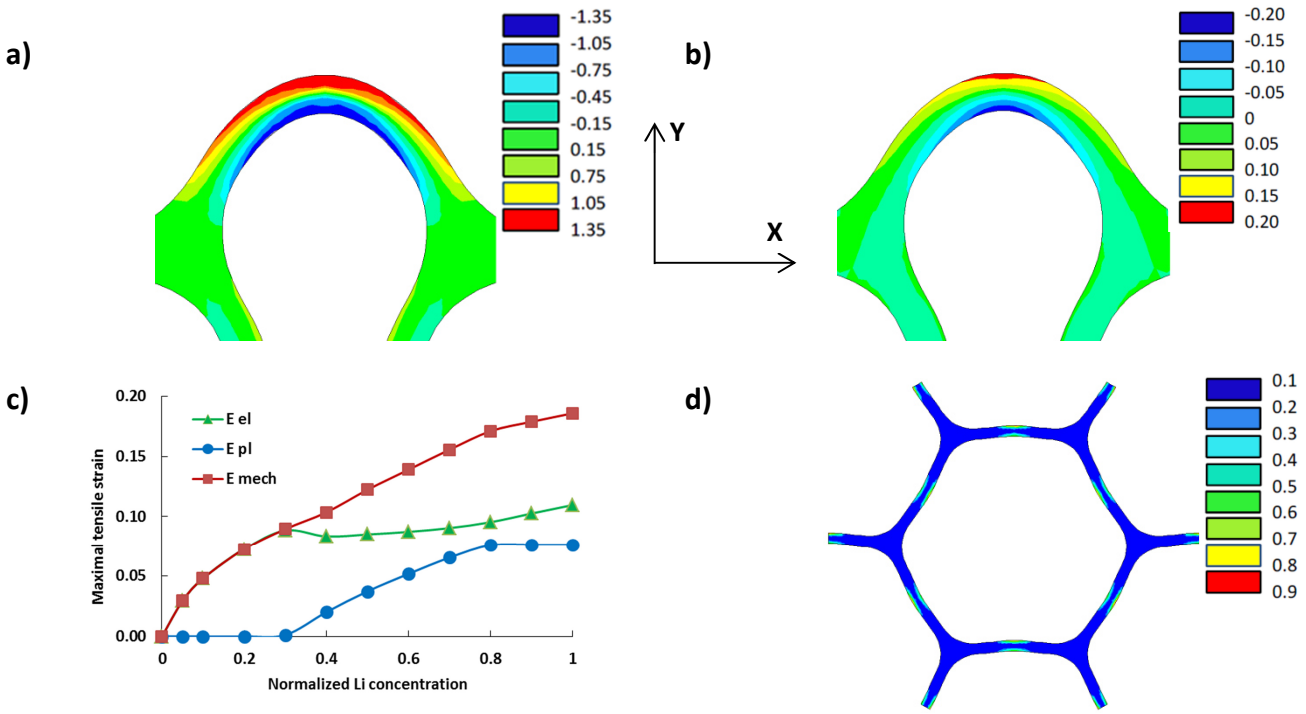

Fig. 3. a-b) Distribution of equivalent stress (a) and equivalent strain (b) across the wall of a fully-lithiated honeycomb; c) Modeled variation of the maximal elastic (E_{el}) and plastic (E_{pl}) strains, and their sum (E_{mech}) in the honeycombs with increasing lithium concentration; d) Modeled honeycomb cell after full lithiation and subsequent full delithiation. The contours show the residual maximal plastic tensile strain.

4. Discussion

The overlay of observed and simulated honeycomb cells shows good agreement between the theoretical and experimental results for 45% and for the maximal achieved experimental Li concentration of 80% (Fig. 1b). Full lithiation up to C_{Li}=1.0 was not reached in the experiments, likely due to the use of amorphous hydrogenated Si as the starting material (α-Si:H), leading to the formation of the LiH phase and solid electrolyte interphase (SEI), thus increasing the losses in charging kinetics [6]. In order to quantify the agreement between modeling and experiments, the displacement at the middle point of six honeycomb walls was determined with respect to their original location by scanning electron microscopy. The simulated and experimental values show good agreement for lithiation of 45 % and 80 % (red markers in Fig. 4a).

Lithiation of honeycombs results not only in wall deflection but also in bending stress in the honeycomb structure. The maximal tensile stress arises on the surface bent outward and at the middle point of its top outer edge (Fig. 3b). This stress is responsible for the maximal tensile strain and fatigue life. We found that maximal tensile stress (first principal stress) is nearly equal to the equivalent (von Mises) stress. Thus, the stress state at this position approaches uniaxial tension. The variation of the maximal tensile stress with lithium content is presented in Fig. 4b. The maximal tensile stress increases rapidly with growing Li content up to approximately C_{Li}=0.2, which is followed by a slow decrease. This development is the result of a decrease in Young's modulus for Si with increasing Li content. The effect of diminishing the Young's modulus is to some extent counterbalanced by the increase in stress due to the growing volume expansion. At C_{Li}=0.3 the maximal tensile stress reaches the current yield strength. During further lithiation up to C_{Li}=0.8, this stress remains equal to the reducing yield strength and correspondingly diminishes with increasing Li content. At larger lithiation the maximal tensile stress becomes lower than the yield strength, leading to only additional elastic deformation.

When the distance between neighboring vertexes doubles ($2L$) the maximal tensile stress is reduced below the yield strength during the whole lithiation cycle. The deformation becomes merely elastic and fully reversible even after full loading up to C_{Li}=1.0 (green curve in Fig. 4b). Nearly the same result is obtained when the honeycomb wall thickness decreases to $0.5t$. Thus, similar to triangular cellular structures discussed before [22], the thickness-over-length ratio (t/L) is a non-dimensional decisive factor for stress and strain in a swelling honeycomb microstructure. A decrease in t/L value leads to a reduction in stress and strain. Besides, a diminishing of t/L factor causes a proportional reduction in the honeycomb footprint-area-specific storage capacity ($S_{f.a.}$). The corresponding value has been estimated from the elementary model of a single honeycomb cell shown in Fig. 4c. The volume of silicon in a single honeycomb cell is determined by $V_{si}=1.5\cdot(L+f)\cdot t \cdot h$, in which $f = L-t/\sqrt{3}$. The footprint area of such a cell is equal to $A_{f.a.}=1.5\cdot\sqrt{3}\cdot L^2$. Thus, the storage

capacity per unit footprint area is calculated by $S_{f.a.}=V_{Si}/A_{f.a.}=1/3\cdot(2\cdot\sqrt{3}-t/L)\cdot t/L\cdot h\cdot C_{Si}$, where C_{si}=8303 mA·h·cm^{-3} is the volumetric storage capacity of Si [6]. Thus, the reference honeycomb structure is characterized by $S_{f.a.}$=88.65 mAh·cm^{-2}. Both structures with size of 2L and 0.5t yield a storage capacity of $S_{f.a.}$=44.89 mAh·cm^{-2}. The loss of nearly one half of the footprint-area-specific storage capacity can be compensated by a proportional increase in height of the honeycomb wall.

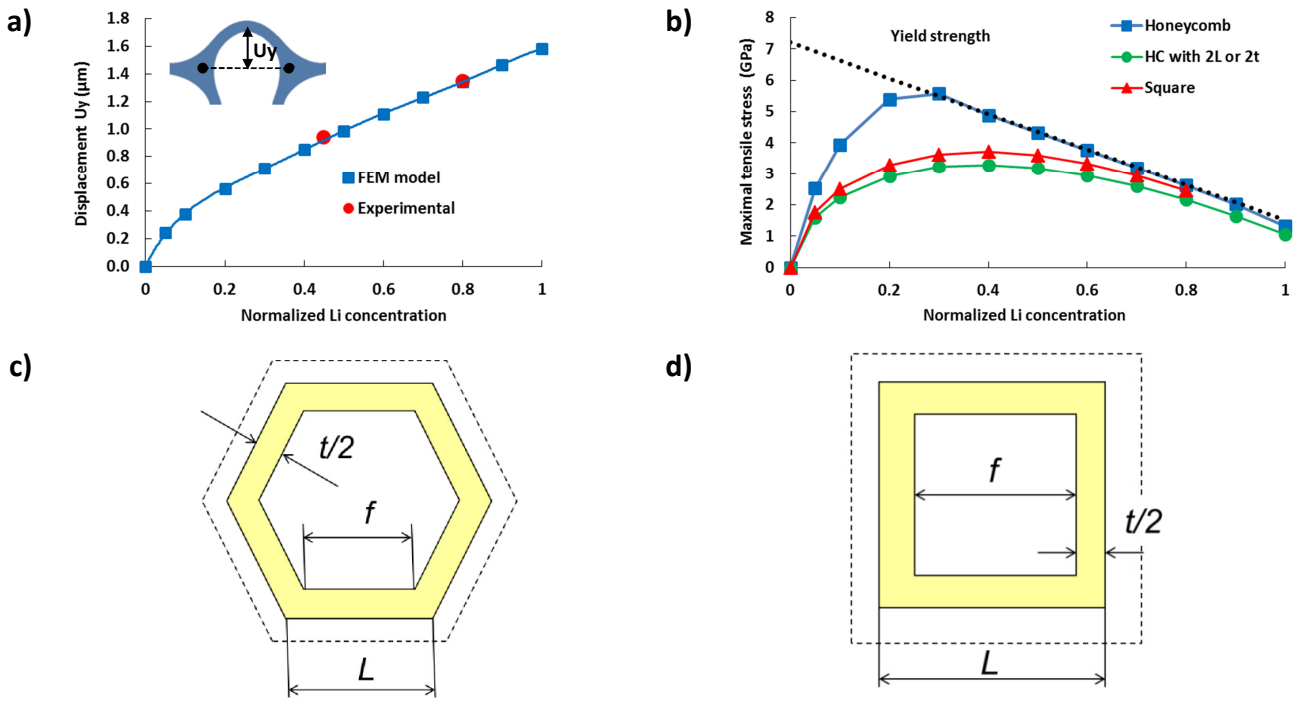

Fig. 4. a) Modeled and experimental displacement of middle point of the honeycomb (HC) wall *vs.* Li concentration; b) Evolution of maximal tensile stress during lithiation of Si with various cellular architectures; c-d) Schematic representation of single cell geometries used to calculate the storage capacity per unit footprint area: c) Honeycomb-based microstructure; d) Square-based microstructure.

Another way of looking at the optimization of micro-structured Si is to use a shape deviating from the honeycombs. A more effective structure should provide a larger distance between two adjacent vertexes than the honeycomb-based structure with the same specific storage capacity per

footprint-area. An interesting option was argued to be the use of square-based Si microstructures as shown in Fig. 4d. The perimeter-to-area ratio (r) for a square is equal to $r=4\cdot L^{-1}$, where L is the distance between neighboring vertexes. This ratio is much lower for honeycombs: $r=2.31\cdot L^{-1}$. This implies that a higher footprint-area-specific storage capacity, which is approximately proportional to r, can be achieved for the square patterns at much larger distances between the adjacent vertexes than in the case of the honeycomb configuration. As noted above, an increase in distance L leads to a favorable decrease in stress during lithiation.

In the present work, we modeled the lithiation of square-structured Si with the same footprint-area coverage, footprint-area specific storage capacity and wall height as for the reference honeycomb-based microstructure. The area of a single square cell is $A=L^2$. This area is assumed to be equal to the area of a reference honeycomb cell. This results in the distance between two neighbouring vertexes in the square-based structure of L=4.674 µm. The volume of Si in a single square cell is given by $V_{si}=(L+f)\cdot t\cdot h$, with $f=L-t$. Correspondingly, the storage capacity per unit of footprint area of square structures is calculated as $S_{f.a}=V_{si}/A=(2-t/L)\cdot t/L\cdot h\cdot C_{si}$. As the height of the walls and the footprint-area-specific storage capacity for both square- and honeycomb-based microstructures are assumed to be identical, this results in a wall thickness of the square cell of t=0.233 µm. Remarkably, our FEM modeling showed that the maximal tensile stress in the square cell is much lower than that in the basic honeycomb cell. This stress level is also always below the yield strength of lithiated Si (Fig. 4b). Therefore, the absence of plastic deformation during the lithiation of a square-based microstructure can be expected. The disadvantage of square patterns is the large wall displacement, leading to collisions of the opposite walls at Li contents slightly above 80% as shown in Fig. 5. This value refers to the maximal theoretical Li content, which can be stored in square-structured Si, which is not a severe limitation due to the high storage capacity of Si. The detailed development of the square-patterned Si microstructure during lithiation is shown in Fig. 5.

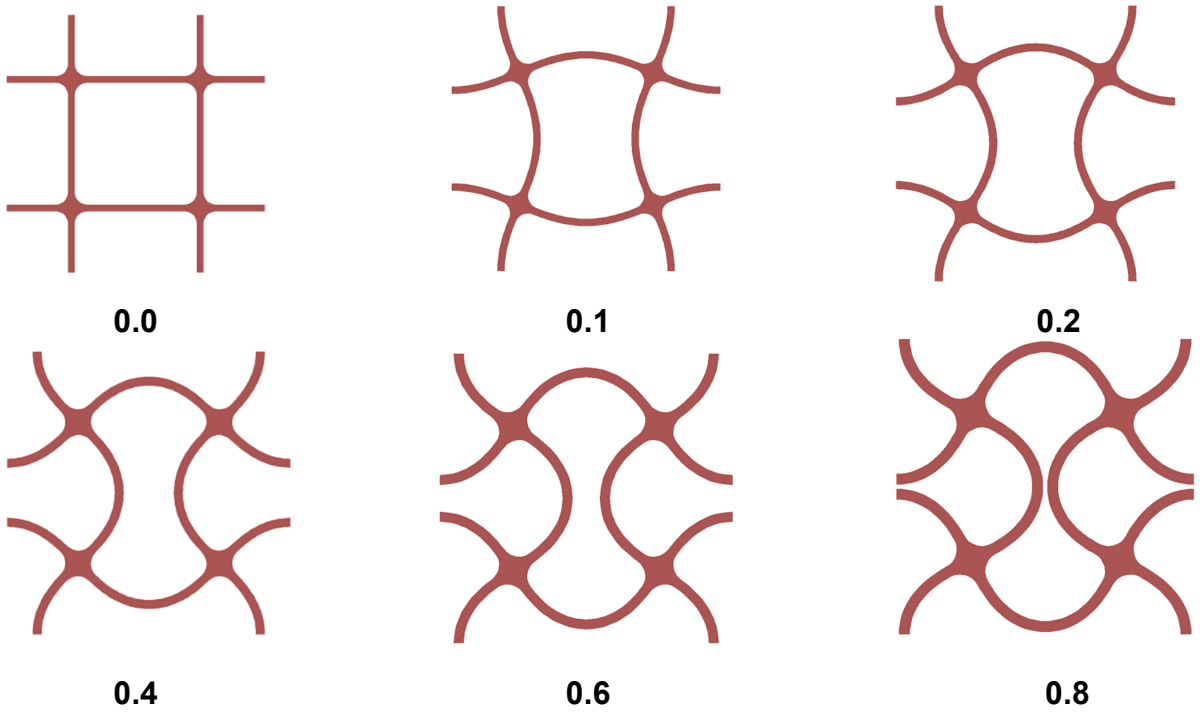

Fig. 5. Modeled evolution of a square Si-cell with increasing lithium content, indicated by the numbers.

5. Conclusions

A finite element model is presented to describe the mechanical behavior of micro-structured Si electrodes upon Li-storage. The model is based on a coupled structural-diffusional analysis of elastoplastic deformation and reveals an excellent capability to predict the large patterned deflection of honeycomb-structured Si. The stress distribution in the severely deformed honeycomb wall is typical for bending and approaches the uniaxial tension/compression state. It was found that with the rise in Li content, the maximal tensile stress at the top of the honeycomb wall first rapidly grows and then diminishes due to the decrease in elastic modulus and yield strength with increasing Li content in Si. Depending on the cell design and material properties, plastic deformation can occur. At high Li content, large plastic strain can significantly influence the geometry of the honeycomb wall, leading to wall buckling and structural collapse. The maximal stress at the top of the wall and associated plastic

strain can be reduced by decreasing the honeycomb wall thickness-to-length ratio. At the same time, the footprint-specific storage capacity of the honeycomb-based cell decreases almost proportionally with reduction of this ratio. The increase in the wall height can compensate this loss in storage capacity. An alternative way to decrease the maximal tensile stress in structured Si is the use of square patterns. However, in this case only approximately 80% Li loading can be allowed due to the large wall displacement, inevitably leading to collisions at higher Li content. This modeling approach can be directly applied to other diffusional processes, which are accompanied with a large volumetric expansion of the host material. The developed finite element method and the used ANSYS® software are shown to be very suitable to simulate the large deformation of ordered, patterned, microstructures under extreme conditions.

References

[1] M. N. Obrovrac, L. J. Krause, Reversible cycling of crystalline silicon powder, J. Electrochem. Soc. **154** (2007) A103–A108.

[2] X. Su, Q. Wu, J. Li, X. Xiao, A. Lott, W. Lu, B. W. Sheldon, J. Wu,. Silicon-based nanomaterials for lithium-ion batteries: A review, Adv. Energy Mater. **4** (2014) 1300882.

[3] H.-C. Shin, J. A. Corno, J. L. Colbe, M. Liu, Porous silicon negative electrodes for rechargeable lithium batteries. J. Power Sources **139** (2005) 314–320.

[4] C. K. Chan, H. Peng, G. Liu, K. McIlwrath, X. F. Zhang, R. A. Huggins, Y. Cui, High-performance lithium battery anodes using silicon nanowires. Nat. Nanotechnol. **3** (2008) 31–35.

[5] M. D. Fleischauer, J. Li, M. J. Brett, Columnar thin films for three-dimensional micro-batteries, J. Electrochem. Soc. **156** (2009) A33–36.

[6] L. Baggetto, R. A. H. Niessen, F. Roozeboom, P. H. L. Notten, High energy density all-solid-state batteries: A challenging concept towards 3D integration, Adv. Funct. Mater. **18** (2008) 1057–1066.

[7] J. Xie, L. Baggetto, D. Danilov, P. H. L. Notten, Silicon anode materials for all-solid-state lithium-ion micro-batteries, TMS 2013 Annual Meeting Supplemental Proceedings, John Wiley & Sons, Inc., Hoboken, New Jersey, 2013, pp. 765–772.

[8] W. W. Troxell, H. C. Engel, Column characteristics of sandwich panels having honeycomb cores, J. Aeronautical Sci. **14** (1947) 413–421.

[9] L. Baggetto, D. Danilov, P. H. L. Notten, Honeycomb-structured silicon: Remarkable morphological changes induced by electrochemical (de) lithiation, Adv. Mater. **23** (2011) 1536–1566.

[10] N. Ding, J. Xua, Y. X. Yao, G. Wegner, X. Fang, C. H. Chen, Determination of the diffusion coefficient of lithium ions in nano-Si, Solid State Ionics **180** (2009) 222–225.

[11] S. Prussin, Generation and distribution of dislocations by solute diffusion, J. Appl. Phys. **32** (1961) 1876–1881.

[12] M. Pharr, Z. Suo, J. J. Vlassak, Variation of stress with charging rate due to strain-rate sensitivity of silicon electrodes of Li-ion batteries, J. Power Sources **270** (2014) 569–575.

[13] M. N. Obrovrac, L. Christensen, Structural changes in silicon anodes during lithium insertion/extraction, Electrochem. Solid-State Lett. **7** (2004) A93–A96.

[14] V. B. Shenoy, P. Johari, Y. Qi, Elastic softening of amorphous and crystalline Li–Si phases with increasing Li concentration: A first-principles study. J. Power Sources **195** (2010), 6825–6830.

[15] B. Hertzberg, J. Benson, G. Yushin, Ex-situ depth-sensing indentation measurements of electrochemically produced Si–Li alloy films, Electrochem. Commun. **13** (2011), 818–821.

[16] A. Kushima, J. Y. Huang, J. Li, Quantitative fracture strength and plasticity measurements of lithiated silicon nanowires by in situ TEM tensile experiments, ACS Nano **6** (2012) 9425–9432.

[17] H. Wang, X. Wang, S. Xia, H. B. Chew, Brittle-to-ductile transition of lithiated silicon electrodes: Crazing to stable nanopore growth, J. Chem. Phys. **143** (2015) 104703.

[18] K. Zhao, W. L. Wang, J. Gregoire, M. Pharr, Z. Suo, J. J. Vlassak, E. Kaxiras, Lithium-assisted plastic deformation of silicon electrodes in lithium-ion batteries: A first-principles theoretical study, Nano Lett. **11** (2011) 2962–2967.

[19] H. Wang, H. B. Chew, Molecular dynamics simulations of plasticity and cracking in lithiated silicon electrodes, Extreme Mech. Lett. **9** (2016) 503-513.

[20] V. A. Sethuraman, M. J. Chon, M. Shimshak, V. Srinivasan, P. R. Guduru, *In situ* measurements of stress evolution in silicon thin films during electrochemical lithiation and delithiation, J. Power Sources **195** (2010) 5062–5066.

[21] V. P. Golub, B. N. Sinaiskii, V. I. Krizhanovskii, Effect of prior plastic deformation and creep strain on fatigue damage for a high-temperature alloy, Strength Mater. **27** (1995) 652-658.

[22] S. H. Kang, S. Shan, A. Košmrlj, W. L. Noorduin, S. Shian, J. C. Weaver, D. R. Clarke, K. Bertoldi, Complex ordered patterns in mechanical instability induced geometrically frustrated triangular cellular structures, Phys. Rev. Lett. **112** (2014) 09870.

Supplementary information

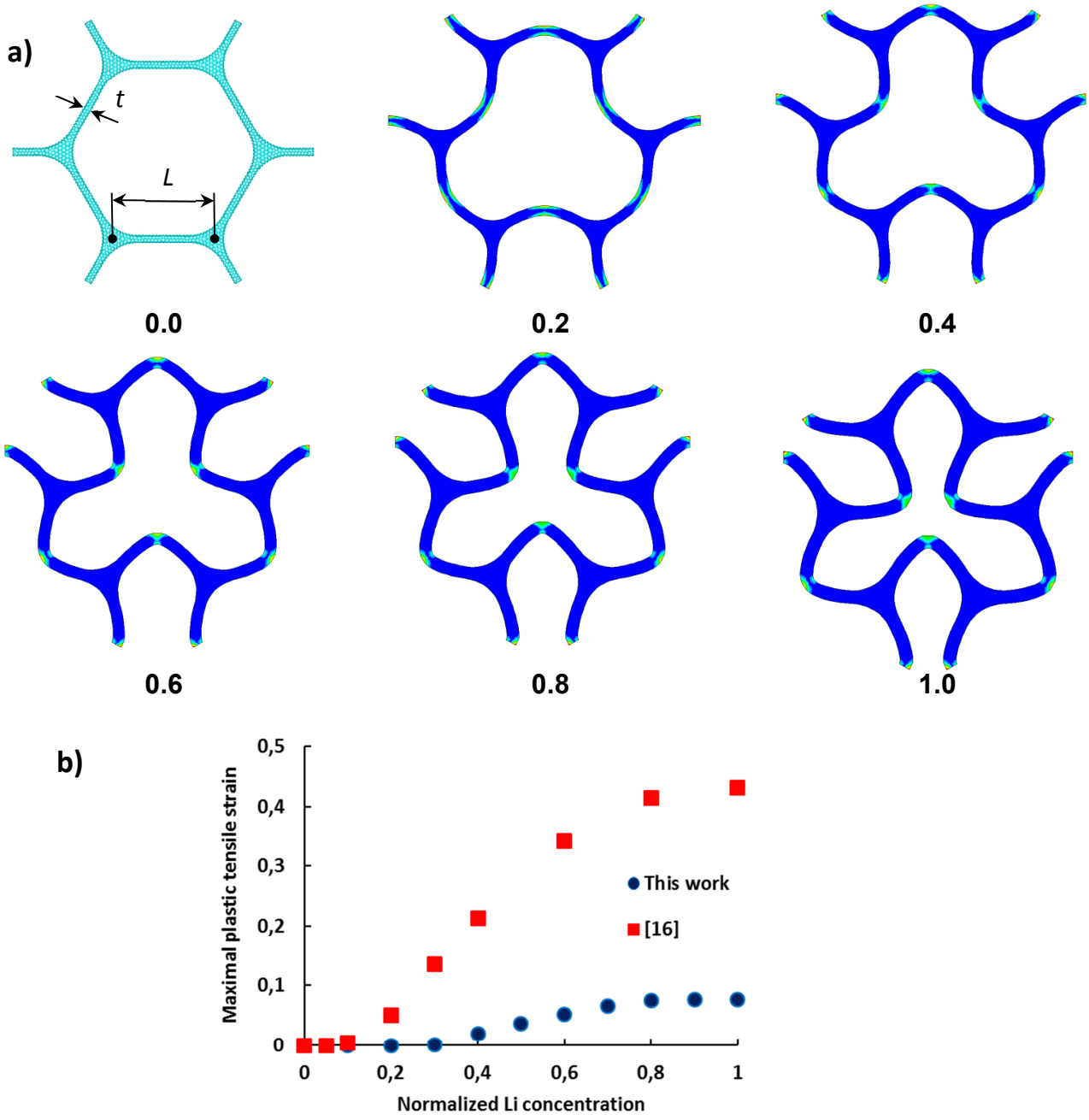

Fig. S1. a) Modeled evolution of a honeycomb cell with increasing lithium concentration (indicated by the numbers) with a yield strength of 3.6 GPa for pristine Si and 0.7 GPa for fully lithiated Si [16]. The contours show the maximal plastic strain penetrating the honeycomb wall; b) Maximal plastic strain evolution modeled with the yield strength used in this work and with that reported for Si nanowires [16].